A Directionally Stable Robotic Sailboat: Concept and Simulations

Jesse Miller
MAE M.Eng. Report, Cornell University

April 2016

Contents

1 Abstract

A conventional, small, autonomous sailboat powered by wind and controlled with solar power may not have enough solar energy to constantly steer itself. At least this is a problem in northern latitudes in winter on overcast days. A potential solution to keeping a sailboat in a desired direction without the use of on-board power is to create a sailboat that is inherently directionally stable. This paper analyzes the directional stability properties of a sailboat using three different types of control surfaces. The directional stability is analyzed using a sailboat simulator created in MATLAB that models the 3D dynamics of a sailboat. A novel control surface, we refer to as a tail, is proposed as a replacement to the conventional rudder in order to improve directional stability of the boat. The tail control surface is attached behind the sail with both the tail and sail independently actuated. Based on tests performed on the simulated sailboats, we find that an actuated sail in conjunction with this tail control surface is ideal for producing a directionally stable sailboat. Thus, it can sail for an extended period of time without the use of electrical power. We present a method for optimizing the design of the sailboat in order to improve the performance of the boat. Finally, we use a model of the sailboat dynamics to produce polar diagrams at various winds speeds. We find that, for a one meter long sailboat with a tail control surface, we are able to sail upwind with directional stability at a velocity made good of $0.30m/s$ in a $5m/s$ wind.

2 Introduction

An unmanned, robotic sailboat is a potential candidate for cheap ocean monitoring and environmental data gathering. Such a sailboat could be powered by nothing more than wind and solar power via solar panels. To reduce the cost per useful data point collected by the boat, these boats should be mass produced while minimizing the size of each boat. However, smaller boats relying on solar power are faced with a power supply problem. Indeed, the available solar power scales with surface area of the hull. However, certain electronic components necessary for a robotic sailboat (such as a GPS) are scale independent [1]. The result is a boat that does not have enough power to constantly steer itself.

In this paper, we examine this problem using a 0.9 meter long, 2 meter tall (ballast to sail tip), 7kg sailboat as a case study. Such a boat would have approximately $0.1m^2$ of space for solar cells which corresponds with an estimated worst case daily average of $0.3W$ of power. This estimate accounts for a solar panel efficiency of about 10%, a 50% loss for bad orientation (due to waves), an 80% loss which accounts for night at high latitudes, and finally a factor of 8 loss from cloud coverage [1]. A boat with an average power supply of $0.3W$ does not have enough power to power various sensors and a computer while also actively controlling the sail and rudder servos. Therefore, for most of the time, the boat will be charging its battery with the solar panels without using the battery's power to steer the boat. The limited time available for steering the boat poses a problem when it comes to navigating the sailboat along a desired trajectory. An analogy to this problem would be trying to drive a car in a straight line while only occasionally being able to use the steering wheel to correct your course.

One of our main goals is to solve this problem by designing a sailboat that can sail with directional stability with respect to the wind. In other words, the sailboat needs to be able to sail in a desired direction without using on-board power to steer the boat. A possible existing solution to this problem would be to

use a mechanical autopilot system, such as a wind vane self-steering system, to maintain a desired heading without consuming power [2]. However, these systems increase the number of moving parts and can decrease the durability of the sailboat.

Our goal is to solve this problem by designing an inherently, directionally stable sailboat. Such a boat has the ability to return to a desired heading regardless of its initial heading and without constantly steering the boat or using a complicated mechanical steering system. Inherent directional stability has also been suggested as a potential solution for an autonomous sailboat with limited on-board power in a conference paper titled, 'Giving Inherent Directional Stability to a Sailing Vehicle' [3]. We propose an inherently directionally stable sailboat design that replaces the traditional water rudder with a control surface, we refer to as a tail, attached to the back of the sail. For this design, both the tail and the sail are independently actuated. Thus, when no power is being used to steer the boat, the sail and tail angles are fixed relative to the hull. This fixed sail and tail design is analogous to the wing and elevator of an airplane.

In this paper we analyze the directional stability of this tail control surface design and compare it to a traditional water rudder design as well as an air rudder attached to the hull of the boat. The directional stability of these designs are quantified by modeling the 3-dimensional dynamics of a sailboat and numerically analyzing the model in a MATLAB simulation.

3 Dynamic Sailboat Model

3.1 Overview

We have created a MATLAB simulation that captures the main aspects that influence the directional stability of the sailboat. In order to create this simulation, a 3D model of the sailboat has been developed. This simulation relies on several assumptions to reduce the overall complexity of the model. For example, the true wind velocity is assumed uniform and the water is assumed to be stagnant with no waves.

Figure 1 shows a labelled diagram of a conventional sailboat. In our model, we break up the sailboat into four main components; the hull, sail, keel, and rudder. The sail, keel, and rudder are treated as airfoils. Note that although the rudder drawn in Figure 1 is a conventional water rudder, this model can easily be modified to capture the dynamics of other types of rudders. The horizontal forces of the hull are modelled using data gathered from a drag test on a one meter long hull. The vertical forces on the hull, such as buoyancy, are modelled by approximating the hull to be an ellipsoid. The specifics of these forces are explained in more detail in the subsequent sections.

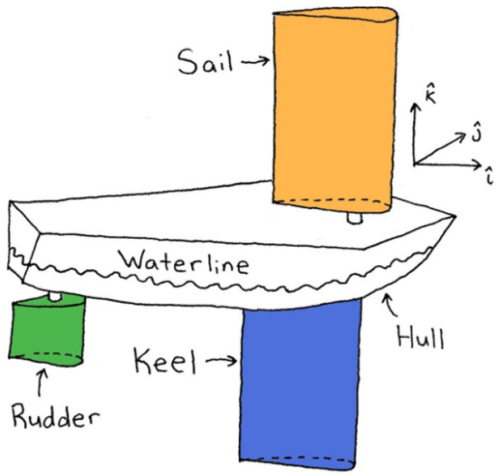

Figure 1: Colored illustration of sailboat where sail, keel, and rudder are represented as airfoils.

These forces are depicted in the free body diagrams, viewed from three different perspectives, shown in Figures 2 to 4. The vectors $\hat{i}$, $\hat{j}$, and $\hat{k}$ represent unit vectors in the fixed inertial frame, $\mathcal{I}$, while $\hat{i}'$, $\hat{j}'$, and $\hat{k}'$ represent unit vectors in the boat or body frame, $\mathcal{B}$. Figure 2 illustrates the leaning or heeling forces (looking at the boat from in front). In this free body diagram, $F_{buoyant}$ is the buoyancy force of the hull, F_{zdamp} is the vertical drag force caused by vertical motion of the hull, F_{sail} and F_{keel} are the resultant lift and drag forces on the sail and keel respectively, and F_{weight} is the net weight of the boat.

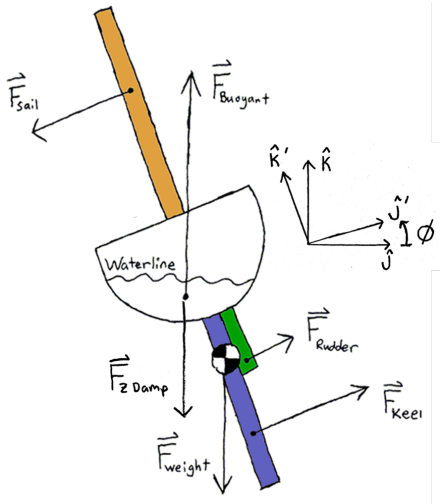

Figure 2: Free body diagram of leaning forces acting on the sailboat.

Figure 3 illustrates the steering forces (looking down on the boat from above). Here, $M_{\Psi damp}$ is the damping moment in the yaw direction and R_{Hull} is the hull resistance.

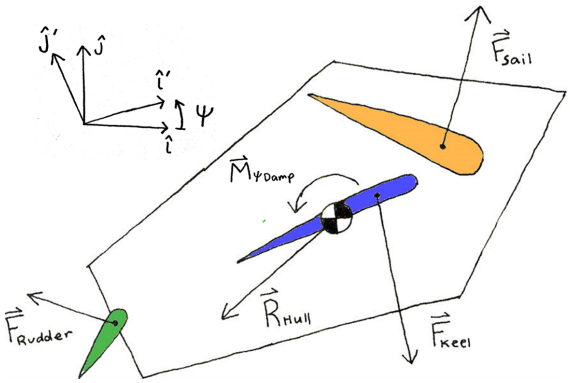

Figure 3: Free body diagram of steering forces acting on the sailboat.

Finally, Figure 4 illustrates the pitching forces (looking at the boat from the side). Here, $M_{\theta damp}$ is the damping moment in the pitch direction and M_θ is restoring moment due to buoyancy.

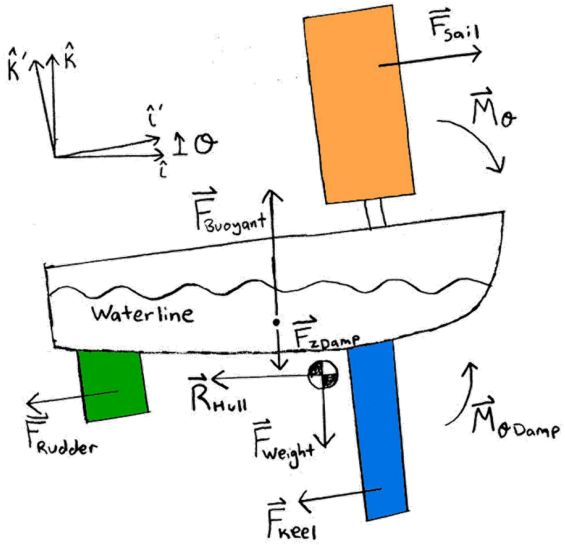

Figure 4: Free body diagram of pitching forces acting on the sailboat.

The boat's orientation is represented using roll ϕ, pitch θ, and yaw Ψ Euler angles in the body frame. Figure 5 shows these Euler angles in the boat frame. This representation allows for a minimum coordinate represent of the orientation of the boat. These 3 angles can also be easily converted into a rotation matrix, $R_{\mathcal{B}}^{\mathcal{I}}$, which is useful for converting forces and moments between the body and the fixed frame. Given these roll, pitch, yaw Euler angles, the rotation matrix can be written as,

$$R_{\mathcal{B}}^{\mathcal{I}} = \begin{bmatrix} c_\Psi c_\theta & c_\Psi s_\phi s_\theta - s_\Psi c_\phi & c_\Psi c_\phi s_\theta + s_\Psi s_\phi \\ s_\Psi c_\theta & s_\Psi s_\phi s_\theta + c_\Psi c_\phi & s_\Psi c_\phi s_\theta - c_\Psi s_\phi \\ -s_\theta & s_\phi c_\theta & c_\phi c_\theta \end{bmatrix} \tag{1}$$

Where s and c represent sin and cos operators respectively [4]. The full state of the boat can thus be written as $\vec{x} = [x_G, y_G, z_G, \phi, \theta, \Psi, \dot{x}_G, \dot{y}_G, \dot{z}_G, p, q, r]^T$ where x_G, y_G, and z_G are the $\hat{\imath}$, $\hat{\jmath}$, and $\hat{k}$ components of the

position of the center of mass, and p, q, and r are the roll, pitch, and yaw angular velocities in the body frame.

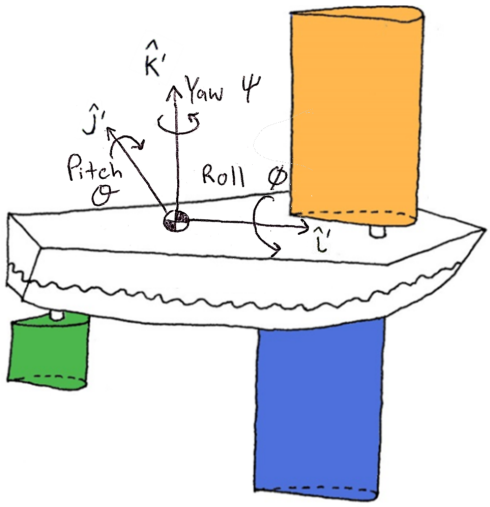

Figure 5: Roll, pitch, yaw angles in boat frame.

Using the Newton-Euler equations, this model can be used to find the equations of motion to determine the 3D dynamics. The linear momentum balance can be written as,

$$\Sigma\vec{F} = m^{\mathcal{I}}\vec{a_G} \tag{2}$$

Where m is the mass of the boat, $\Sigma\vec{F}$ is the sum of the force vectors shown in the free body diagrams, and ${}^{\mathcal{I}}\vec{a_G}$ is the acceleration vector of the center of mass of the boat in the inertial frame. By dotting equation 2 with the unit vectors $\hat{i}$, $\hat{j}$, and $\hat{k}$ in the fixed frame, the translational equations of motion can be determined,

$$\ddot{x_G} = \hat{i} \cdot (\Sigma\vec{F}/m) \tag{3}$$

$$\ddot{y_G} = \hat{j} \cdot (\Sigma\vec{F}/m) \tag{4}$$

$$\ddot{z_G} = \hat{k} \cdot (\Sigma\vec{F}/m) \tag{5}$$

Where $\ddot{x_G}$, $\ddot{y_G}$, and $\ddot{z_G}$ are the $\hat{i}$, $\hat{j}$, and $\hat{k}$ components of the acceleration of the center of mass respectively.

Angular momentum balance is used calculate the rotational equations of motion. The angular momentum balance for the 3D dynamics of a rigid body in the principle orthogonal coordinate frame (which, due to symmetry, is approximately the body fixed frame shown in figure 5) reduces to,

$$\dot{p} = \frac{\hat{i}' \cdot (\Sigma\vec{M_G}) + (I_{yy} - I_{zz})qr}{I_{xx}} \tag{6}$$

$$\dot{q} = \frac{\hat{j}' \cdot (\Sigma\vec{M_G}) + (I_{zz} - I_{xx})pr}{I_{yy}} \tag{7}$$

$$\dot{r} = \frac{\hat{k'} \cdot (\Sigma \vec{M}_G) + (I_{xx} - I_{yy})pq}{I_{zz}} \tag{8}$$

Where $\dot{p}$, $\dot{q}$, and $\dot{r}$ are the $\hat{i'}$, $\hat{j'}$, and $\hat{k'}$ components of the angular velocities in the body frame respectively. I_{xx}, I_{yy}, and I_{zz} are the body-fixed principle moments of inertia and $\Sigma \vec{M}_G$ is the sum of the moments about the center of mass of the boat represented in the body frame [4].

The angular velocities in the body frame; p, q, and r can be related to the angular velocities in the inertial frame; $\dot{\phi}$, $\dot{\theta}$, and $\dot{\Psi}$ using Equation 9 to 11,

$$\dot{\phi} = p + (q\sin(\phi) + r\cos(\phi))\tan(\theta) \tag{9}$$

$$\dot{\theta} = q\cos(\phi) - r\sin(\phi) \tag{10}$$

$$\dot{\Psi} = (q\sin(\phi) + r\cos(\phi))/\cos(\theta) \tag{11}$$

Equations 3 to 11 can be used to calculate the time derivative of the state vector, $\dot{\vec{x}}$ [4]. Using $\dot{\vec{x}}$, the state of the boat is numerically solved using MATLAB's ode45 function. This numerical solution provides the motion of the boat used in the simulation.

3.2 Forces on the Sail, Keel, and Rudder

Since the sail, keel, and rudder are modeled as airfoils, the net force on each airfoil, $\vec{F}_{airfoil}$, can be broken up into lift, $\vec{L}$, and drag, $\vec{D}$, forces,

$$\vec{F}_{airfoil} = \vec{L} + \vec{D} \tag{12}$$

The magnitude of the drag force can be written as,

$$|\vec{D}| = \frac{1}{2} C_D \rho_{fluid} S |\vec{v}_{app}|^2 \tag{13}$$

Where C_D is the drag coefficient, ρ_{fluid} is the density of the fluid that airfoil is in (e.g. air density for the sail), S is the reference area, and $\vec{v}_{app}$ is the apparent fluid velocity that the airfoil experiences.

Similarly, the magnitude of the lift force can be written as,

$$|\vec{L}| = \frac{1}{2} C_L \rho_{fluid} S |\vec{v}_{app}|^2 \tag{14}$$

Where C_L is the lift coefficient.

The coefficients of lift and drag are a function of the angle of attack of the airfoil, α, and are interpolated from data from a NACA 0015 airfoil as can be seen in figure 6 [5]. The piecewise cubic hermite interpolating polynomial (PCHIP) MATLAB function was found to accurately capture the features of C_L and C_D without being overly computationally expensive. Note that parasitic drag was added to C_D so that $max(\frac{C_L}{C_D}) \approx 5$. The location where the lift and drag forces act along the airfoil is modelled as moving from the quarter-chord from the front to the quarter-chord from the back as the angle of attack increases from 0° to 180°.

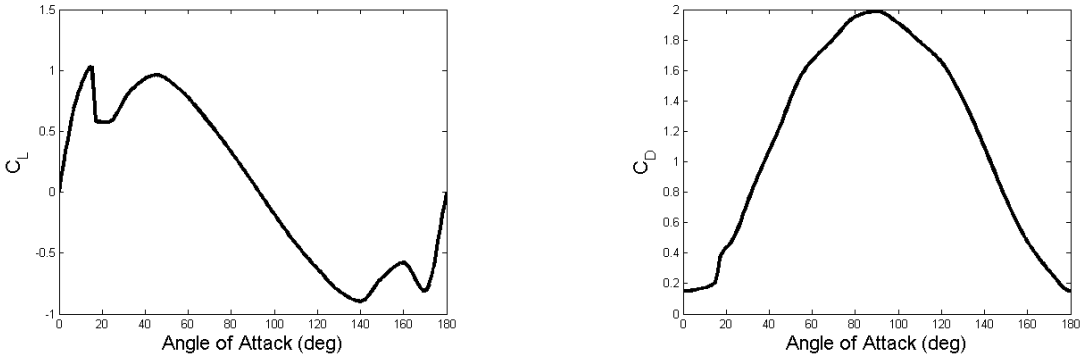

Figure 6: Interpolated lift (left) and drag (right) coefficients for a NACA 0015 airfoil vs. angle of attack

The coefficient of drag in Figure 6 is for an airfoil of infinite span. Since the sail, keel, and rudder are airfoils of finite span, they will experience an additional drag force caused by the downwash at the tip of the airfoil. This additional drag coefficient is referred to as induced drag and can be calculated for a rectangular airfoil as,

$$C_{Di} = \frac{C_L^2}{0.7\pi AR} \tag{15}$$

Where AR is the aspect ratio of the airfoil [6]. The total drag coefficient for the finite airfoil $C_{Dfinite}$ is thus,

$$C_{Dfinite} = C_D + C_{Di} \tag{16}$$

Due to the boat's combined translational and rotational motion, the $\vec{v}_{app}$ profile along the airfoil may not be uniform in magnitude or direction. Blade element theory is used in the simulation to account for this. Using blade element theory, an airfoil (in this case sail, keel, or rudder) is divided lengthwise into n elements. Each element is treated as its own airfoil with unique C_L and C_D values. The $\vec{v}_{app}$ for the center of each element is individually calculated by combining the translational, inertial velocity of the boat's center of mass ${}^{\mathcal{I}}\vec{v}_{boat}$, the inertial velocity of the fluid ${}^{\mathcal{I}}\vec{v}_{fluid}$, and the inertial velocity caused by the boat's rotational velocity,

$${}^{\mathcal{I}}\vec{v}_{app} = -{}^{\mathcal{I}}\vec{v}_{boat} + {}^{\mathcal{I}}\vec{v}_{fluid} - {}^{\mathcal{I}}\vec{\omega}^{\mathcal{B}} \times \vec{r}_{/G} \tag{17}$$

Where ${}^{\mathcal{I}}\vec{\omega}^{\mathcal{B}}$ is the angular velocity of the boat and $\vec{r}_{/G}$ is the position vector of the center of the blade element relative to the center of mass of the boat. Once $\vec{v}_{app}$ is calculated for each element along the airfoil, values for $\vec{L}$ and $\vec{D}$ forces can be calculated for each segment and then combined to get the net force on the airfoil.

The number of blade elements n is a parameter in the simulation. For increased accuracy, n can be increased but at the expense of added computation time. As an example, figure 7 shows the lean angle of the boat over time for a boat that is oscillating back and forth. The number of blade elements n used in the simulation

is varied. This figure shows that as n is increased, the simulation converges. However, unless $\vec{\omega}_{boat}$ is very large, a value of $n = 1$ is sufficient for most analysis purposes.

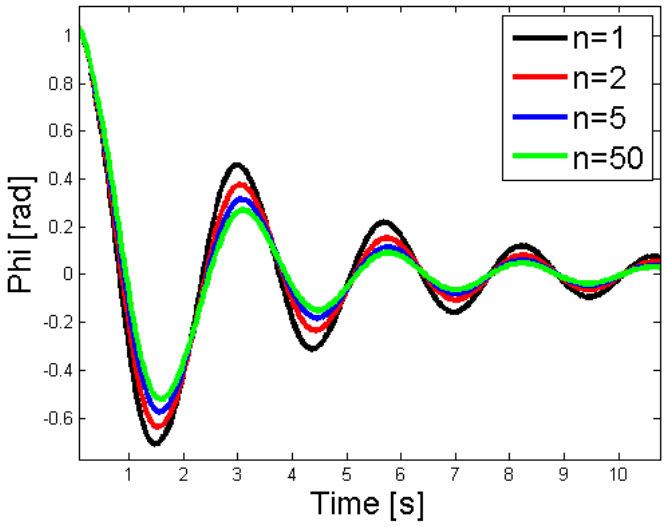

Figure 7: Simulated lean angle of the boat vs. time using 1, 2, 5, and 50 blade elements to calculate the forces on the sail, keel, and rudder.

3.3 Hull Resistance

While the rudder, keel, and sail are modeled as airfoils, the complex shape of the hull requires experimental data to model. The hull resistance, $\vec{R}_{hull}$, depends on several factors such as the shape of the hull, the weight of the boat, and the velocity of the boat. A simple experiment was performed to determine the relationship between the hull resistance and boat velocity. Two 1 meter long boats were pulled through the water using a pulley system and the velocity of the boat was recorded. Four different weights were used to pull the boat and each weight was used for three tests on each boat. Based on the 24 data points gathered from the experiment (2 boats times 4 weights times 3 tests per weight), a cubic regression was fit to the data shown in Figure 8. This regression relates the hull resistance and boat velocity as follows,

$$\vec{R}_{hull} = -C_{reg}|\vec{v}_{boatxy}|\vec{v}_{boatxy} \tag{18}$$

Where $C_{reg} = 6.5[kg{\cdot}s/m^2]$ is the regression coefficient and $\vec{v}_{boatxy}$ is the velocity vector of the boat projected on the local $\hat{i}$, $\hat{j}$ plane. Not only does the hull experience the quadratic drag, similar to the airfoil, it also experiences wave-making resistance. Therefore, a cubic relation between $\vec{R}_{hull}$ and $\vec{v}_{boatxy}$ makes qualitative sense. While the cubic regression accurately represents the experimental data, it may diverge for larger values of $\vec{v}_{boatxy}$. However, since the velocities of the boat during the experiment fall within the expected velocity range of the boat, this regression is sufficient to model the hull resistance. It is also assumed that $\vec{R}_{hull}$ is in the opposite direction of $\vec{v}_{boatxy}$ and its magnitude is independent of the orientation of the boat. This is not an accurate assumption. The magnitude of $\vec{R}_{hull}$ will, of course, be larger when angle between $\vec{v}_{boatxy}$ and

the boat's heading is increased. However, the force on the keel will replicate this effect by increasing drag for lateral motions.

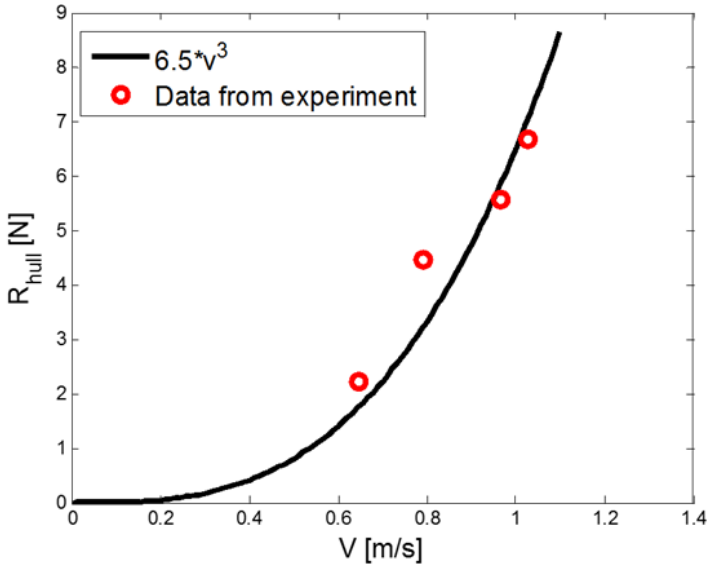

Figure 8: Experimental hull resistance data versus boat velocity with a cubic regression applied

The location of $\vec{R}_{hull}$ acts at the center of pressure of the hull. This location is modelled as varying between the quarter chord point from the bow to the quarter chord point from the stern as the angle of attack of the hull increases from 0° to 180°. This center of pressure variation is modelled after that of an airfoil which has its center of pressure at about the quarter chord location for small values of α, at the center-chord location for $\alpha = 90°$, and quarter chord location from the back when α nears 180°.

Hull damping moments, $\vec{M}_{\Psi damp}$ and $\vec{M}_{\theta damp}$, were added in the $\hat{k}'$ and $\hat{j}'$ directions respectively. These moments capture the rotational damping forces that the water exerts on the hull. To approximate these damping moments, the hull is modelled as a cylinder with quadratic drag. The quadratic drag force on a cylinder, $\vec{F}_{dragCyl}$ is,

$$|\vec{F}_{dragCyl}| = \frac{1}{2} C_d D_{hull} L_{hull} \rho_{water} v^2 \tag{19}$$

Where $C_d \approx 1$ is the drag coefficient of a cylinder, D_{hull} and L_{hull} are the diameter and length of the hull respectively, and v is the velocity of the hull in the water [6]. We then estimate the velocity of the hull as the linear velocity of the stern and bow caused by the hull's rotational velocity. The location of this force is then approximated as acting at the end of the stern and bow. From these assumptions, the resulting damping moments are,

$$\begin{aligned} \vec{M}_{\theta damp} &= -\frac{1}{16} C_d D_{hull} L_{hull}^4 \rho_{water} q|q| \\ \vec{M}_{\Psi damp} &= -\frac{1}{16} C_d D_{hull} L_{hull}^4 \rho_{water} r|r| \end{aligned} \tag{20}$$

Note that these damping moments affect the transient, not the steady-state, response of the system. Since we are mostly interested in the steady state sailing of the boat, getting these moments exactly right is not

a priority.

3.4 Buoyancy Model for the Hull

The buoyancy force of the hull is important as it can provide both transverse and longitudinal stability to the boat. The buoyancy force can be written as,

$$\vec{F}_{buoyancy} = \rho_{water} V_{sub} g \hat{k} \tag{21}$$

Where ρ_{water} is the density of water, V_{sub} is the submerged hull volume, and g is the acceleration due to gravity.

Calculating $\vec{F}_{buoyancy}$ requires knowing the submerged hull volume, V_{sub}. In order to reduce the run-time of the simulation and reduce the complexity of the analysis, the hull shape can be approximated as an ellipsoid. The submerged hull volume as a function of draft is calculated analytically using a double integral between the waterline and the ellipsoid symbolically in MATLAB. However, a sinusoidal approximation almost perfectly matches the analytic submerged volume as seen in Figure 9. Due to the improved computing time and close approximation, the sine estimation was chosen to be used in the model. This sine approximation can be written as,

$$V_{sub} = \frac{V_{tot}}{2}(1 - cos(\frac{\pi d}{2c})) \tag{22}$$

Where V_{tot} is the total volume of the ellipsoid, d is the draft of the hull, and c is the semi-axis length of the ellipsoid along the vertical direction.

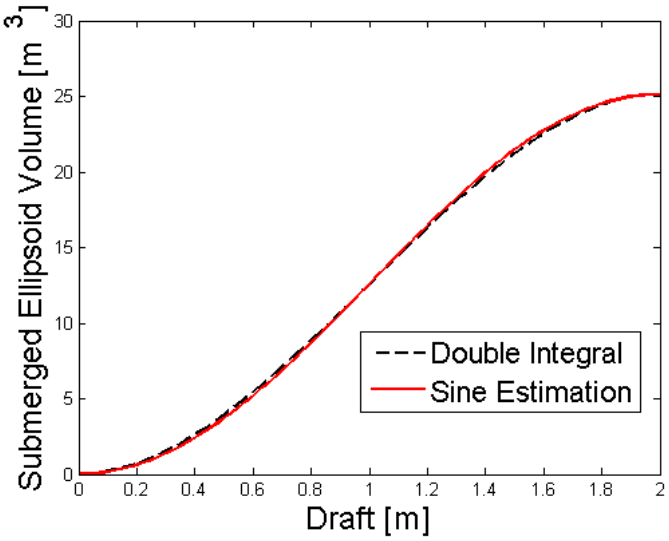

Figure 9: Submerged hull volume vs. Draft. Comparison between analytic value and sine approximation.

The buoyancy force is also responsible for providing longitudinal stability to the boat. At a small pitch angle, the buoyancy force provides a restoring moment which acts to bring the boat back to an upright position.

Figure 10 shows the a simplified figure of a hull, looking at if from the side. The sub-figure on the left shows the upright hull where the buoyant and weight forces act along the same line, causing no net moment. The sub-figure on the right shows a hull with a small pitch angle. In this figure, the change in the waterline from AB to CD causes the center of volume, and thus the location of $F_{Buoyant}$, to shift location resulting in a moment about the center of mass that acts to stabilize the boat. In other words, the change in the waterline from AB to CD adds submerged volume on one side (shown in green) and subtracts submerged volume on the other (shown in red). Therefore, the pitching moment due to buoyancy, M_θ, is found by calculating the net moment caused by the change in the submerged volume distribution. For small angles of θ, the net pitching moment is,

$$\vec{M}_\theta = -I_{Area}\rho_{water}g\theta\hat{j}' \tag{23}$$

Where I_{Area} is the second moment of area of the waterplane section [7].

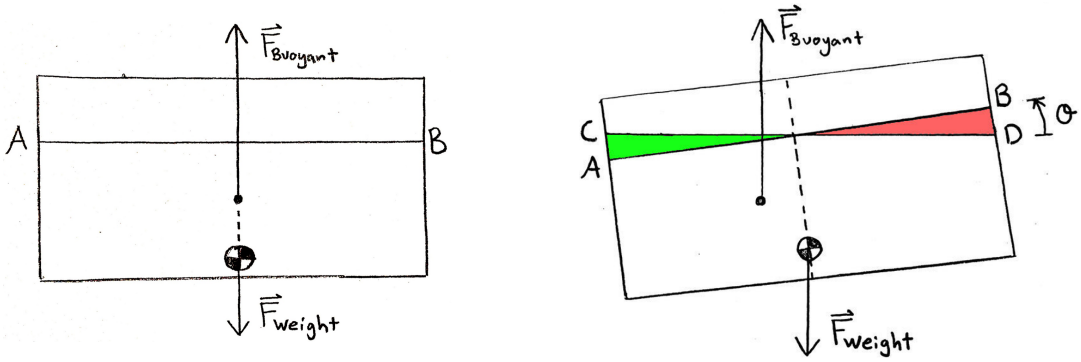

Figure 10: Left: Side view of hull where line AB represents the waterline. $F_{Buoyant}$ and F_{Weight} act along the same line. Right: Side view of hull with a small pitch angle θ. New waterline is represented by line CD. The gained submerged volume is highlighted in green while the lost submerged volume is highlighted in red.

4 3D Sailboat Simulation

MATLAB's ode45 function was used to find the trajectory of the boat over time based on the modeled forces and moments on the boat. A parameter file, setBoatParam.m, allows for the initial conditions and various parameters to be defined before running the simulation. These parameters include the dimensions, masses, and relative locations of the sail, keel, and rudder. The weights of ballast and hull can also be selected as well as the size of the hull. True wind velocity can also be selected in this parameter file.

Once the desired parameters have been selected, running the main.m file executes the simulation. Figure 11 shows a screen-shot of the simulation which animates the trajectory of the boat.

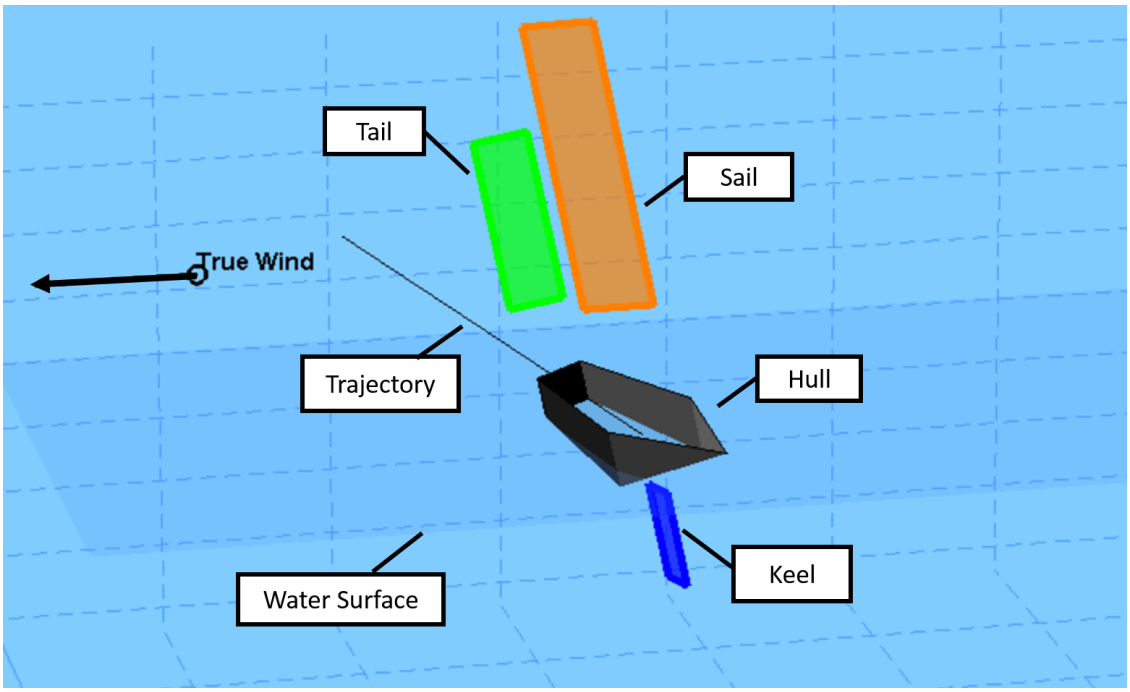

Figure 11: Screen-shot of animation from the sailboat simulation. Annotations show locations of sail, keel, rudder (in this case tail), hull, water surface, and true wind direction.

5 Directional Stability

5.1 Directional Stability Requirements

The main motivation for creating the 3D sailboat simulation is to test and compare the directional stability of various sailboat designs. As previously mentioned, a variety of factors are taken into consideration when evaluating the directional stability of a sailboat.

1. We want a sailboat that is able to sail in a desired direction regardless of the initial conditions of the boat (i.e. initial velocity and orientation). For instance, if the boat orientation is disturbed by a strong gust of wind, the boat should be able to return to its original direction without actively steering.

2. Another valuable characteristic of directional stability is that small disturbances in the various parameters affecting the boat do not cause large changes in the trajectory of the boat. For instance, if the actual angle of the rudder is a few degrees off of the desired angle, the resulting trajectory of the boat should not be more than a few degrees off of the desired path.

3. Finally, we want a sailboat that has a wide range of stable directions, both upwind and down wind. Indeed, a directionally stable boat would have limited functionality if it were only stable when sailing upwind.

5.2 Types of Control Surfaces Tested

The main purpose of the control surface is to produce a moment about the boat to control the heading. Typically, a rudder located in the water is used as the control surface of a sailboat. The direct ability of the rudder to steer the boat makes it an important factor when improving directional stability. Three types of control surface designs were tested in the simulation to determine their stability properties. Each type of control surface is assumed to be actuated (e.g. by a servo motor). Since we are interested in the stability of the boat when no on-board power is consumed, the control surfaces are treated as having a constant angle relative to the object to which they are attached.

1. **Water Rudder:** The water rudder is the traditional control surface for steering a sailboat. The rudder is attached to the stern of the hull and is located under water. Figure 12 illustrates the water rudder placement.

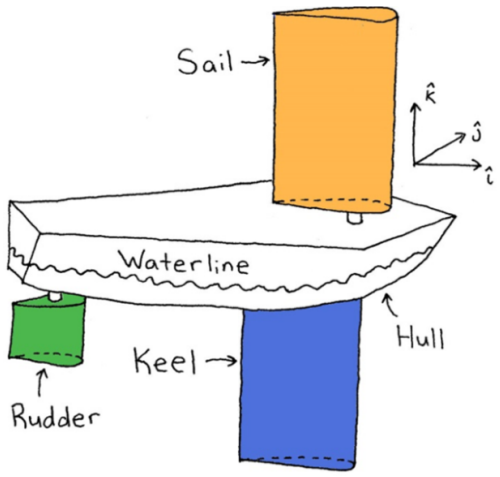

Figure 12: Illustration of sailboat using water rudder control surface

2. **Air Rudder:** The second type of rudder is an air rudder. This rudder is the same as the water rudder except the rudder is located in the air as seen in Figure 13.

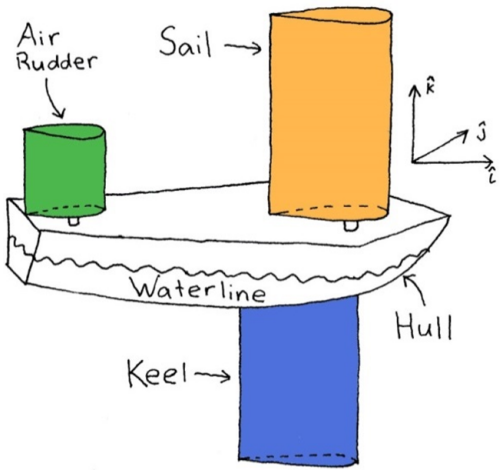

Figure 13: Illustration of sailboat using air rudder control surface

3. **Tail:** The third type of control surface is referred to as a tail and is attached directly to the sail as seen in Figure 14. The reason we refer to this control surface as a tail is because it is has similar characteristics to the tail of an airplane, where the position and angle of the tail is relative to the main wing (sail). In other words, this tail will remain behind the trailing edge of the sail and its angle will change relative to the sail's angle. This novel control surface concept has been designed with the purpose of increasing the directional stability of the sailboat. Although this tail can be actuated, we wish to examine the stability of the tail when no on-board power is consumed. Thus, the simulation assumes that the tail remains at a fixed angle relative to the sail for the duration of the simulation.

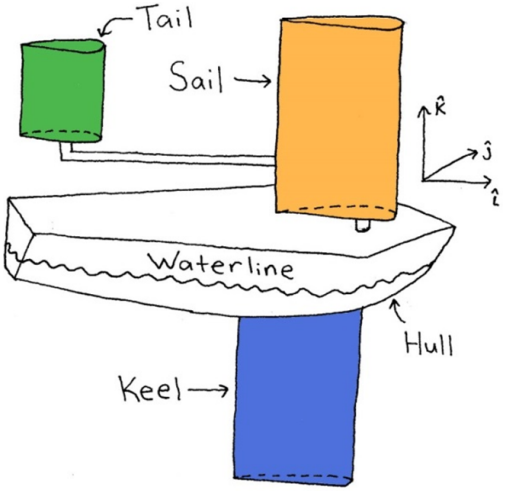

Figure 14: Illustration of sailboat using tail control surface

5.3 Results of Directional Stability Test

The simulation was run for a variety of trails. For each trial, the boat parameters were changed in order to improve the directional stability of the boat. The results of these trials were used to make qualitative and

Table 1: Parameters used in the simulation to test the directional stability of the sailboat.

True Wind Speed		$5\ m/s$	**Ballast Mass**		$1.1\ kg$
Sail	**Chord Length**	$0.24\ m$	**Water rudder**	**Chord Length**	$0.1\ m$
	Span	$1\ m$		**Span**	$0.1\ m$
	Mass	$0.66\ kg$		**Mass**	$0.4\ kg$
	Distance in front of C.O.M.	$0\ m$		**Distance in front of C.O.M.**	$-0.4\ m$
Keel	**Chord Length**	$0.04\ m$	**Air rudder/ Tail**	**Chord Length**	$0.18\ m$
	Span	$0.68\ m$		**Span**	$0.46\ m$
	Mass	$0.3\ kg$		**Mass**	$0.04\ kg$
	Distance in front of C.O.M.	$0\ m$		**Distance in front of C.O.M.**	$-0.4\ m$

quantitative conclusions about the directional stability of various boat designs.

The following results were obtained by modelling a $0.9m$ long and $7kg$ sailboat in the simulation. These results were obtained using the parameters shown in Table 1. Some of these parameters were varied slightly during the simulation to determine their effect on the directional stability. Since the main factor that affects the directional stability of the boat is the type of control surface, the directional stability of each control surface is analyzed and discussed separately. Note that the simulation neglects water currents and waves.

5.3.1 Water Rudder

The actuated water rudder failed to meet all of the desired directional stability properties. Attempting to find a stable sailing direction typically results in an inefficient or unstable sailing trajectory. Figure 15 plots an example, unstable trajectory of the sailboat. These conditions were produced by setting the sail angle to 130° and the rudder angle to 10° relative to the hull. Since we are interested in the stability when no on-board power is consumed, these angles are held constant throughout the simulation.

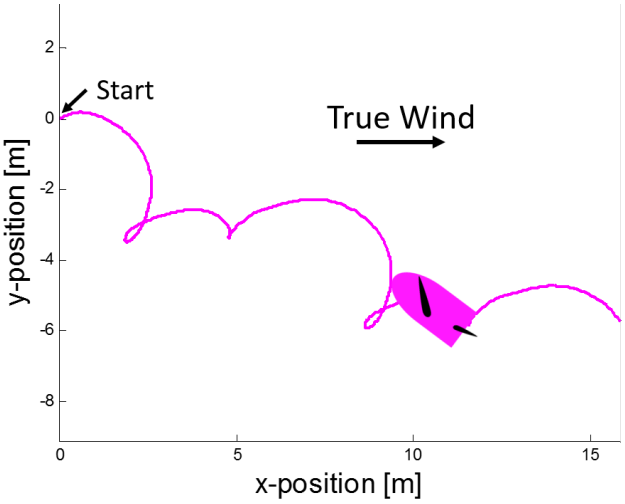

Figure 15: Example of an unstable sailing trajectory caused by using a water rudder control surface. An illustration of the boat (including the hull, sail, and rudder) is plotted along this trajectory.

Not all of the trajectories were unstable when using the water rudder. Indeed, certain sail and rudder angles resulted in stable sailing directions. However, the stability of these directions was not robust. For example, Figure 16 shows how a small disturbance in the rudder angle of 6° causes nearly a 180° change in the stable sailing direction of the boat. This indicates that the stable trajectory of the boat is overly sensitive to disturbances in the rudder angle. Due to this sensitivity, the water rudder design fails to meet all of the desired stability criteria.

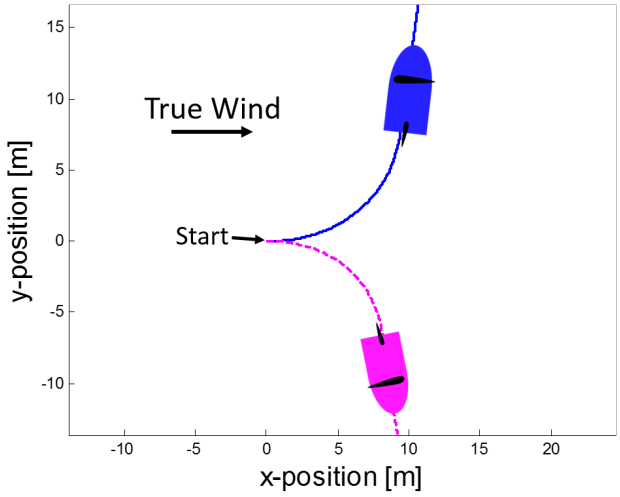

Figure 16: Sailboat trajectories produced by two separate trials using the water rudder. The rudder angle between the trials was varied by 6°. The results indicate that the stable sailing direction is very sensitive to disturbances in the rudder angle.

5.3.2 Air Rudder

Directional stability independent of initial orientation was achieved using the air rudder combined with the actuated (fixed) sail. An example of the directional stability of the air rudder and actuated sail is shown in Figure 17. The parameters listed in Table 1 were used and the angle of the sail and rudder with respect to the boat were set to 40° and 60° respectively. The simulation was run for three trials, varying the initial boat heading in each. The change in the direction of the boat trajectory over time and the trajectory of the boat for each trial are shown in Figure 17. The air rudder produced directional stability that was independent of the initial orientation of the boat.

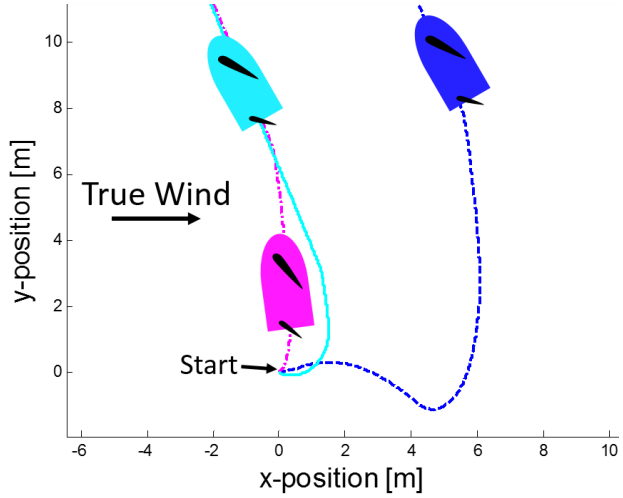

Figure 17: Sailboat trajectories produced by three separate trials using the air rudder control surface. The initial orientation of the sailboat was varied for each trial. The results indicate that the stable sailing direction is independent of the initial orientation.

While the air rudder was able to achieve directional stability independent of its initial orientation, it was found to have a limited range of stable directions. In order for the sailboat using the air rudder to reach a stable direction, the resultant center of pressure on the sail and air rudder has to be downwind of the center of mass of the boat. In this case, a small disturbance in boat direction would result in an aerodynamic restoring moment on the sail/air rudder system. However, if the resultant center of pressure were in front of the center of mass, then a small disturbance causes the boat to become unstable. Therefore, depending on the positions of the sail and air rudder relative to the center of mass, the sailboat only has stable directions when sailing upwind or downwind but not both. Due to the limited range of stable sailing directions, the air rudder fails to satisfy all of the desired characteristics of directional stability.

5.3.3 Tail Control Surface

Unlike the water and air rudders, the tail control surface combined with the actuated (fixed) sail was able to satisfy all of the desired characteristics of directional stability. The air rudder was only able to achieve a limited range of stable directions since the center of pressure of the rudder/sail system did not move relative to the boat. However, unlike the air rudder, the tail control surface is fixed to the back of the sail. Therefore,

as the sail rotates, the tail rotates behind it. By shifting location of the center of pressure of the sail/tail system, the boat is able to achieve stable trajectories both upwind and downwind. Figure 18 illustrates this qualitatively. Since the sail and keel both act at the center of mass, the tail provides the main moment that turns the boat. Therefore, the tail will steer the boat such that the tail becomes roughly in-line with the relative wind direction. Any small disturbance from this equilibrium will result in a restoring moment from the tail which causes this trajectory to be stable.

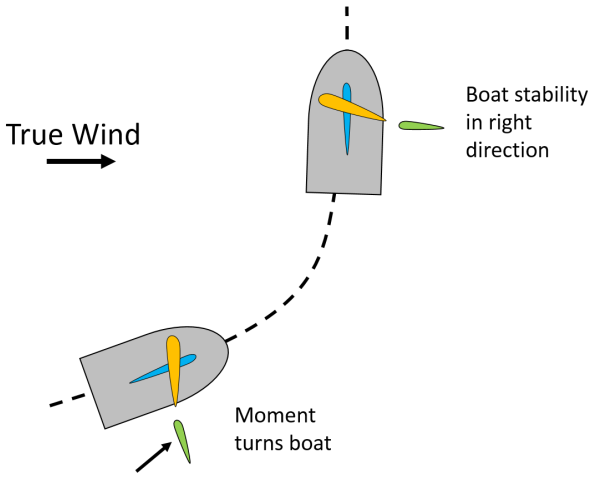

Figure 18: Qualitative illustration of a force on tail resulting in a directionally stable trajectory.

The tail control surface design was tested in the simulation to determine whether it satisfied the desired directional stability properties. For the first test, the simulation was run for three trials where the initial boat heading was varied. This test was designed to determine whether the sailboat would return to the same stable direction regardless of initial orientation. Figure 19 shows that the sailboat was, indeed, able to return to the desired heading regardless of its initial orientation.

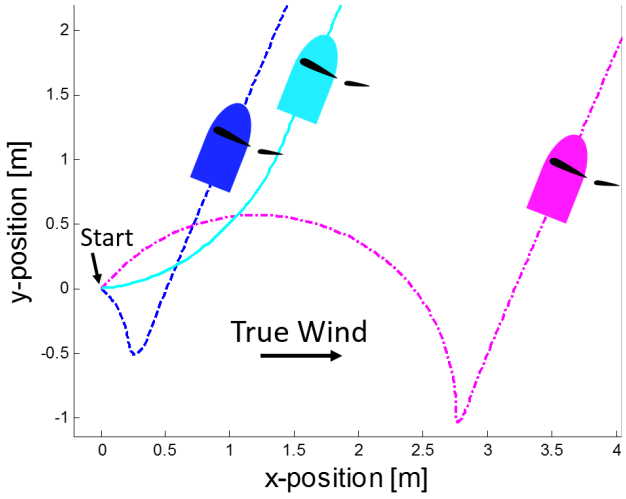

Figure 19: Sailboat trajectories produced by three separate trials using the tail control surface. The initial orientation of the sailboat was varied for each trial. The results indicate that the stable sailing direction is independent of the initial orientation.

A second test was performed in the simulation to determine whether small disturbances in the parameters of the sailboat would have a large effect on the direction of stability. This test involved changing the angles of the sail and tail $\pm 0.1 rad$ to determine the effect on the overall trajectory of the boat. The results show that a $\pm 0.1 rad$ change in sail and tail angles corresponds with about a $\pm 0.1 rad$ change in the stable direction of the boat, as seen in figure 20. This one-to-one correspondence between the boat parameters and angle of stability is expected. Since both the keel and the sail are located near the center of mass of the boat, the moment caused by the tail is the primary moment steering the boat. The tail will, thus, provide a moment on the boat until the tail is aligned parallel to the apparent wind. Therefore, if the angle of the tail is changed by $0.1 rad$, the boat will also change direction by $0.1 rad$ so that the tail is realigned with the apparent wind. Since the angle of the tail is relative to the sail, a $0.1 rad$ change in the sail angle will have this same effect.

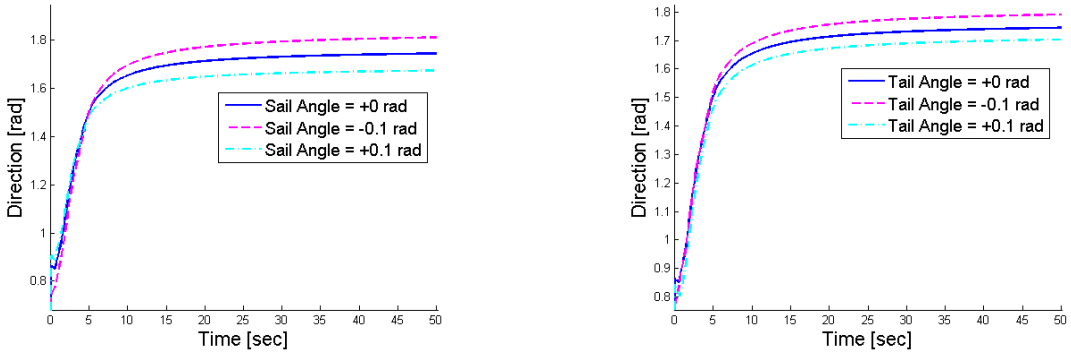

Figure 20: (Left) Effect on the stable direction of the boat when changing the sail angle by $\pm 0.1 rad$. (Right) Effect on the stable direction of the boat when changing the tail angle by $\pm 0.1 rad$.

A test was also performed to confirm that the sailboat can sail with directional stability both upwind and downwind. Figure 21 shows three separate trials run in the simulation where the sailboat was able to achieve trajectories downwind, perpendicular to the wind, and upwind.

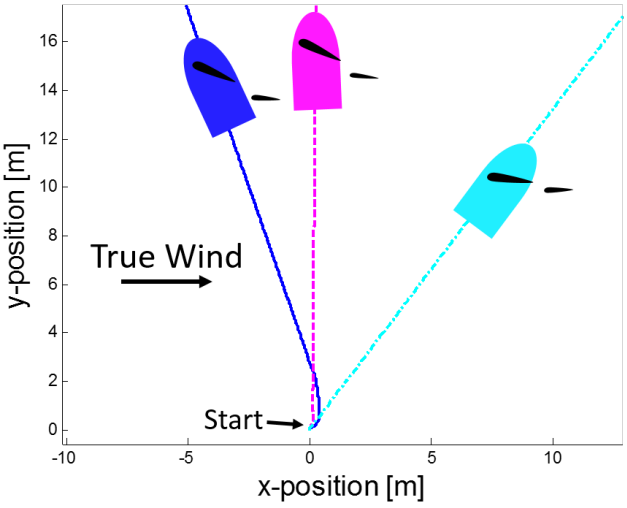

Figure 21: Trajectory of the sailboat over three trials using a tail control surface. Results show a range of stable directions both upwind and downwind.

So far, we have shown that the tail control surface design is successful in making the sailboat directionally stable. However, when strong winds increase the heeling of the boat, we have found that multiple stable solutions may occur. This is not a desirable result, since this indicates that the stable direction of the boat depends on its initial condition. For instance, a disturbance could cause a boat sailing along a desired, stable trajectory to switch to an alternative stable direction. Figure 22 shows sailing trajectories for two separate trials with the sail and tail angles at 100° and 15° respectively. These trajectories exhibit this dual stable direction phenomenon. The green trajectory is the desired stable direction while the red trajectory is newly formed stable direction due to the large heeling angle of the boat. The heel angle is also plotted for each trajectory. The heel angle for the desired trajectory demonstrates oscillatory motion, indicating neutral stability. The undesired trajectory has a heel angle that decays to a constant value, which indicates more robust stability.

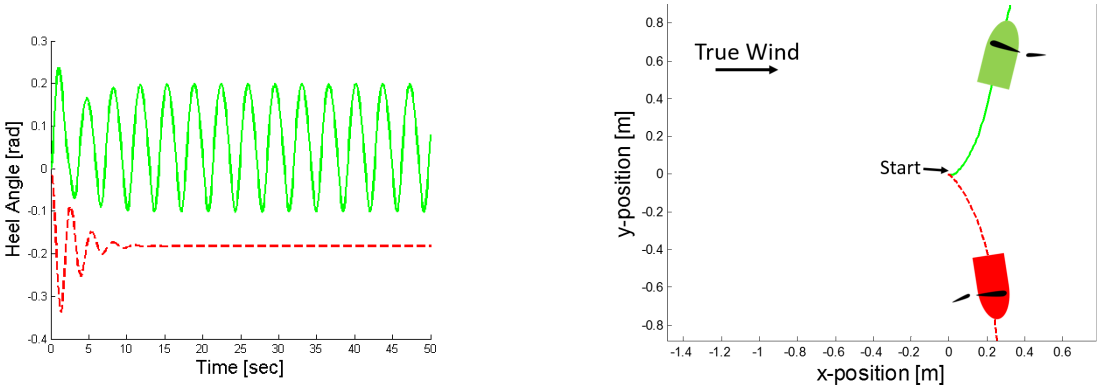

Figure 22: (Left) Heeling angle of the boat corresponding to the two stable trajectories illustrated in the figure to the right. (Right) Sailing trajectories for two separate trials using the tail control surface. For each trial, the boat has the same sail and tail angles but starts at a different orientation. The results show that multiple stable directions exist due to the higher heel angle.

Figure 23 attempts to qualitatively explain the existence of multiple equilibrium solutions. The figure on the left shows the sailboat sailing along the desired stable direction. In this configuration, the center of pressure of the tail and sail system is downwind of the center of pressure of the underwater forces. Note that this solution occurs even when there is no heeling angle because the tail is positioned downwind of the sail. Any disturbance from this equilibrium results in the tail exerting a restoring moment indicating that this is a stable equilibrium. The figure on the right shows the other stable equilibrium that occurs due to the large heel angle of the boat. In this configuration, the tail is actually located upwind from the sail. This solution could not be stable if the boat was upright because a disturbance from the equilibrium would cause the tail to produce a destabilizing moment. However, because the boat is heeling, the force from the sail acts downwind of the underwater center of pressure. This means that it is possible for the stabilizing moment produced by the sail force to dominate the destabilizing moment from the tail.

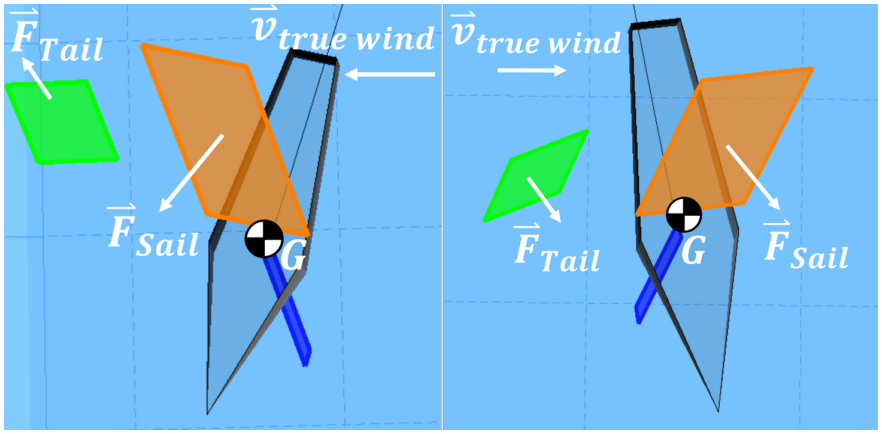

Figure 23: (Left) Screenshot of the animation showing the sailboat sailing at the desired stable trajectory. (Right) Screenshot of the animation showing the sailboat sailing at the stable trajectory caused by excessive healing of the boat.

Because multiple stable solutions arise from the boat heeling, this issue can be prevented by reducing the heel angle. Various design changes will reduce the lean angle such as increasing the ballast weight or reducing the height of the sail. More research is required better understand the phenomenon of multiple stable solutions and to determine other options for preventing them.

6 Optimizing Sailboat with Tail Design

So far, we have shown that the tail control surface design satisfies all of the desired directional stability criteria. However, we have not yet described how to choose the dimensions of the tail, or other aspects of the boat design, in order to construct a boat with good performance characteristics. We now wish to optimize the boat design in order to improve its performance. More specifically, we are interested in determining the ideal chord length and span of the sail, keel and tail as well as the distance of the tail behind the sail. Since the tail control surface is a novel concept, we do not simply have the option of basing our boat on existing boat designs. Therefore, we have developed a method for estimating the optimal design of the boat using a nonlinear optimization function in MATLAB, FMINCON.

The FMINCON optimization function attempts to minimize a cost function, subject to linear and or nonlinear constraints. Since we are interested in optimizing the performance of the boat, we must first define a cost function that quantitatively defines some aspect of the boat's performance. A potential metric for defining the boat's performance is to use the overall speed of the boat at a given true wind speed. Maximizing the overall boat speed is equivalent to maximizing the area within the boat's polar plot. However, maximizing a polar plot is computationally expensive as it requires optimizing the boat's speed at various sailing directions. A simpler metric that provides an estimate of the overall boat speed is the boat's velocity made good, or VMG. VMG is a measure of the component of the boat's velocity in the direction of the true wind. While VMG does not directly measure the overall performance of the boat, a boat that can sail upwind faster tends to sail in other directions faster as well. We can write the velocity made good as,

$$VMG = -\vec{V}_{boat} \cdot \frac{\vec{V}_{trueWind}}{|\vec{V}_{trueWind}|} \tag{24}$$

Where $\vec{V}_{boat}$ and $\vec{V}_{trueWind}$ are the boat and true wind velocities respectively. Therefore, we define the cost function as $-VMG$ since minimizing the cost function will result in maximizing VMG.

We want to ensure that the VMG is optimized under steady state sailing conditions. This constraint can be implemented in FMINCON as a nonlinear constraint. The steady state sailing constraint implies that the translational and rotational acceleration components of the boat's dynamics are zero,

$$\begin{aligned} \ddot{x}_G &= 0 \\ \ddot{y}_G &= 0 \\ \ddot{z}_G &= 0 \\ \dot{p} &= 0 \\ \dot{q} &= 0 \\ \dot{r} &= 0 \end{aligned} \tag{25}$$

The translational and rotational accelerations are calculated based on the dynamic model described in section 3.

As previously mentioned, the optimization function requires variable parameters to optimize in order to minimize the cost function. In this case, we have chosen to optimize the chord length and span of the sail, keel, and tail as well as the distance of the tail behind the sail. Bounds on these parameters are also set to ensure the optimized dimensions can be manufactured and meet structural requirements.

In addition to the cost function and nonlinear constrain, several constraints have been added to ensure that the optimized solution is reasonable. Indeed, without any additional constraints, the optimized solutions may not produce a functional sailboat. For instance, the optimization algorithm may make the surface area of the tail zero to minimize the air drag. It could still find an equilibrium solution that maximizes the VMG. However, this design would not produce a functional sailboat since it is unable to steer without a tail control surface.

To ensure that tail is large enough to steer the boat, the moment due to the lift force on the tail must overwhelm the moment due to the lift force on the sail. The moment arm length between the sail and keel

center of pressure, δ, varies as their respective angles of attack change during turning shown in Figure 24. Assuming that the center-line of the sail and keel are aligned, the maximum δ will be,

$$\delta = (L_s + L_k)/4 \tag{26}$$

Where L_s and L_k are the chord lengths of the sail and keel respectively [8]. This center of pressure misalignment occurs when the sail center of pressure is at the quarter chord location from the front and the keel center of pressure is at the quarter chord location from the back, or vice versa. Since we wish to ensure that the tail moment can counteract the sail moment, we set the tail moment greater than or equal to the tail moment about the center of pressure of the keel. Assuming that the relative wind velocity and angle of attack for the sail and tail are similar, this moment balance simplifies to Andy's Law,

$$A_s(\frac{Ls + L_k}{4}) \leq A_t l \tag{27}$$

Where l is the distance of the center of pressure of the tail behind the center of pressure of the keel and A_s and A_k are the areas of the sail and tail respectively [8]. Using Andy's Law, with a safety factor of 2, as an addition constraint in the optimization function ensures that the tail control surface will be large enough to steer the boat.

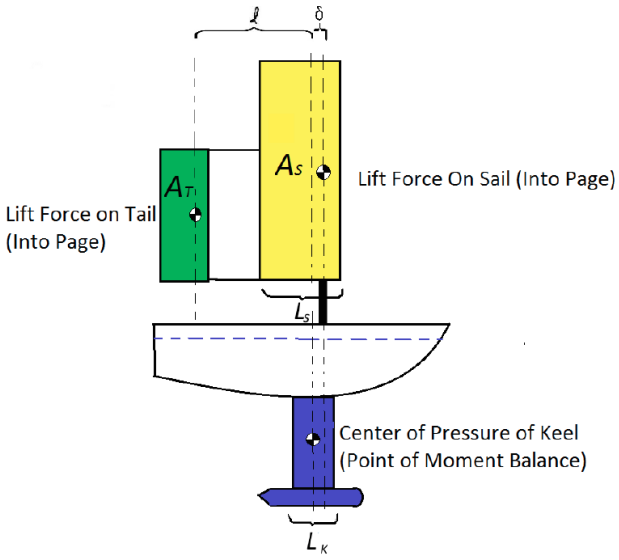

Figure 24: Moment balance about the center of pressure of the keel [8]

Another nonlinear constraint is added to ensure the boat will have leaning stability by enforcing that the center of mass is below the center of buoyancy. Additional linear constraints include enforcing that the height of the boat, from the ballast to the top of the sail, remains within $2m$ and that the chord lengths of the sail and tail are not so long that they interfere with each other.

Running this nonlinear constrained optimization problem, produces the optimal chord length and span for the sail, keel, and tail as well as the length of the sail behind the tail. These optimized parameters are listed in Table 1.

7 Polar Diagrams for the Sailboat with Tail Design

A polar diagram is a plot showing the boat speed versus course angle relative to a given true wind speed and direction. A polar diagram provides a method for evaluating the performance of the boat at various wind speeds. Here, we will analyze the polar diagrams for this 1 meter long sailboat using a tail control surface in order to estimate the feasibility of sailing this boat at various wind speeds.

To generate the polar diagrams for the sailboat with tail design, we use the same FMINCON optimization function described in section 6. The polar plot is generated by varying the course angle from 0° to 180° relative to the true wind. For each course angle, the sail and tail angles are optimized to maximize the boat velocity in that direction. Thus, the cost function is simply the negative of the magnitude of the boat's velocity, $-|\vec{v}_{boat}|$. The resulting maximum velocities and corresponding course angles are plotted as the radial and angular components of a polar plot respectively.

Figure 25 shows the polar diagram for the sailboat using a tail control surface with the optimized dimensions shown in Table 1. Recall that the dimensions of the boat have been optimized for a true wind speed of $5m/s$. The polar diagram reveals several interesting properties of the sailboat. For instance, as the true wind speed increases, the minimum angle that the boat can sail into the wind decreases. Indeed, for true wind speeds of $10m/s$, $5m/s$, and $2m/s$, the boat was able to sail into the wind at a minimum angle of 65°, 55°, and 45° respectively. This reduction in the boat's ability to sail upwind is caused by increase in heeling at higher wind speeds. As the boat leans more, the lift force on the sail loses its component in the direction of the boat's heading and gains a component in the vertical direction. In fact, the maximum velocity made good for this boat occurs at a wind speed of $5m/s$ rather than $10m/s$, with a value of $VMG = 0.30m/s$.

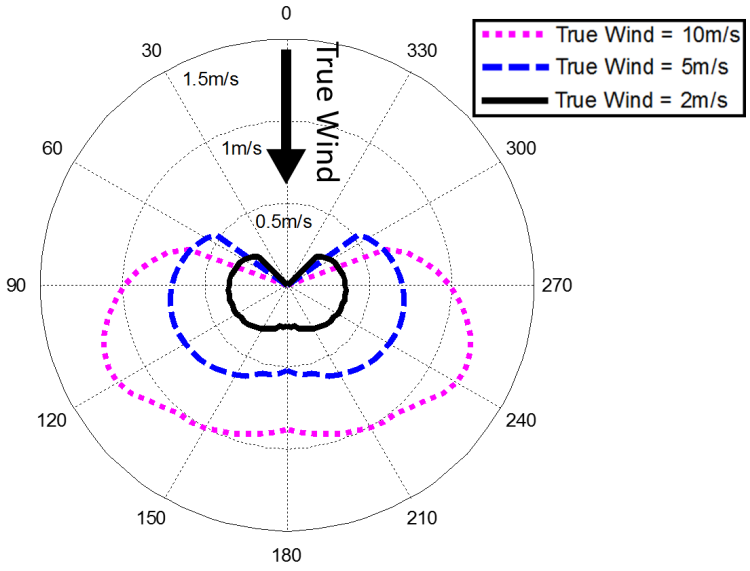

Figure 25: Polar diagram at various wind speeds. Polar diagram is generated for a 1 meter long sailboat using a tail control surface with the parameters optimized for a $5m/s$ wind speed shown in Table 1.

The results of this polar diagram confirm that the sailboat with tail design can sail upwind for a range of wind speeds. Due to the decrease in upwind sailing performance for faster wind speeds, it is important

to optimize the boat's design for realistic wind speed conditions. For instance, this boat design has been optimized for a wind speed of $5m/s$ which means that the upwind sailing performance starts to deteriorate for wind speeds greater than $5m/s$. It should also be noted that these polar diagrams were generated with the assumption of placid water (no waves). Indeed, the affect of waves would act to further reduce the upwind sailing speed of the boat.

8 Conclusions

Tests performed in a MATLAB 3D dynamic sailboat simulation confirm the directional stability of the sailboat with tail control surface design. In the simulation, this sailboat design was able to achieve a desired stable sailing direction regardless of the initial orientation of the sailboat. A second test confirmed that small disturbances in the sail and tail angle had equally small effects on the direction of stability, indicating that the stable sailing direction is not overly sensitive to input noise. The sailboat was also able to achieve a range of stable trajectories both upwind and downwind. In conditions causing a large heeling angle of the boat, we found that multiple stable sailing directions emerged. Some options to prevent this problem include lowering the center of mass of the boat and or reducing the height of the sail. However, future work is required to better understand and prevent this phenomenon.

The FMINCON optimization function was used to optimize the 1 meter long sailboat with tail design for a $5m/s$ wind. The polar diagram for this boat indicates that a maximum upwind velocity made good of $0.30m/s$ can be achieved at true wind speed of $5m/s$. The polar diagram also revealed that higher wind speeds reduce the boat's ability to sail upwind. These results indicate that if the sailboat is expected to experience wind speed greater than $5m/s$, the boat design should be re-optimized for such a wind speed.

9 Future Work

Now that a physical sailboat has been constructed with the tail design, experiments can be carried out with the physical sailboat to validate the sailboat simulation. Furthermore, tests can be performed on the physical sailboat to use as more accurate data for the simulation. For instance, hull drag caused by lateral motions of the hull could be added to the simulation by running experiments on the current hull design.

The current sailboat simulation can also be made more robust. For example, the effects of waves on the sailboat performance can be added to the simulation. Ocean waves may have a strong impact on the directional stability of the sailboat and should be included in the simulation. Furthermore, the sail and tail are currently assumed to both experience the free stream relative wind speeds. However, in reality, the flow upstream of the tail is disturbed by the sail. This induced flow could have a significant effect on the performance of the tail.

References

[1] Andy Ruina. Nri: Low-cost robotic sailboats for long-term ocean monitoring, March 2016.

[2] Optimization problem. http://www.selfsteer.com/index.php.

[3] A. Sakurai, N. Maeda, and Y. Makise. Giving inherent directional stability to a sailing vehicle. *International Society of Offshore and Polar Engineers*, 4, 2002.

[4] Jeremy Kasdin Derek Paley. *Engineering Dynamics A Comprehensive Introduction*. Princeton University Press, 2011.

[5] Jeff Scott. Airfoils at high angle of attack. http://www.aerospaceweb.org/question/airfoils/q0150b.shtml, 2002.

[6] Nancy Hall. Induce drag coefficient. https://www.grc.nasa.gov/www/k-12/airplane/induced.html.

[7] Brian Trenhaile. Understanding ship and boat stability. http://hawaii-marine.com/templates/stability_article.htm, September 2005.

[8] Thomas Augenstein. Using a tail to control an autonomous sailboat, December 2015.